LITERATURE CITED

Abe, I., K. Hayashi, M. Kitagawa, and T. Urahata, "Adsorptive Mechanism on Activated Carbon in the Liquid Phase," *Bull. Chem. Soc. Jap.*, **53**, 1199 (1980).

Altshuler, G., and G. Belfort, "Selective Adsorption of Organic Homologues onto Activated Carbon from Dilute Aqueous Solutions: III. Branching and Predictions," Am. Chem. Soc. Nat'l Mtg., Atlanta (March 28, 1981).

Belfort, G., "Selective Adsorption of Homologues onto Activated Carbon from Dilute Aqueous Solutions. Solvophobic Interaction Approach: II. Development and Test of Theory," *Chemistry in Water Reuse*, **2**, W. J. Cooper, Ed., Ann Arbor Science, Ann Arbor, MI (1981a).

Belfort, G., "Similarity of Ideal Adsorbed Solution and Potential Theories for Adsorption from a Bulk Phase onto a Solid Surface," *AIChE J.*, **27**, 1021 (1981b).

Defay, R., I. Prigogine, A. Bellemans, and D. H. Everett, Translator, "Surface Tension and Adsorption," John Wiley and Sons, New York (1966).

Freundlich, H., *Colloid and Capillary Chemistry*, Methuen and Co., Ltd. London (1926).

Halicioglu, J., and O. Sinanoglu, "Solvent Effects on Cis-Trans Azobenzene Isomerization," *Ann. N.Y. Acad. Sci.*, **158**, 308 (1969).

Horvath, C., W. Melander, and I. Molnar, "Solvophobic Interactions in Liquid Chromatography with Nonpolar Stationary Phases," *J. Chrom.*, **125**, 129 (1976).

Leo, A., P. Y. C. Jow, C. Silypo, and C. Hansch, "Calculation of Hydrophobic Constant (Log P) from π and f constants," *J. Med. Chem.*, **18**(9), 865 (1975).

Manes, M., "The Polanyi Adsorption Potential Theory and its Applications to Adsorption from Water Solution onto Activated Carbon," *Activated Carbon Adsorption of Organics from Aqueous Phase*, **1**, Ann Arbor Science (1980).

Manuf. Chemists Assoc. Research Project, Chemical Thermodynamics Properties Center, "Selected Values of Properties of Chemical Compounds," Texas A&M University, College Station (1966).

McBain, J. W., *The Sorption of Gases and Vapors by Solids*, George Routledge & Sons, Ltd., London (1932).

McGuire, M. J., I. H. Suffett, and J. V. Radziul, "Assessment of Unit Processes for the Removal of Trace Organic Compounds from Drinking Water," *J. Am. Water Works Assoc.*, **70**, 565 (1978).

McGuire, M. J. and I. H. Suffett, "The Calculated Net Adsorption Energy Concept," *Activated Carbon Adsorption of Organics from the Aqueous Phase*, **1**, Ann Arbor Science (1980).

Miller, S., "Adsorption on Carbon: Solvent Effects on Adsorption," *Environ. Sci. Technol.*, **14**(8), 910 (1980a).

Miller, S., "Adsorption on Carbon: Solvent Effects on Adsorption," *Environ. Sci. Technol.*, **14**(9), 1037 (1980b).

Quayle, O. R., "The Parachors of Organic Compounds," *Chem. Revs.*, **53**, 439 (1953).

Reid, R. C., J. M. Prausnitz, and T. K. Sherwood, "The Properties of Gases and Liquids," McGraw-Hill, New York (1977).

Sinanoglu, O., "Solvent Effects on Molecular Associations," *Molecular Associations in Biology*, B. Pullman, Ed., Academic Press, New York 427 (1968).

Sinanoglu, O., "The Solvophobic Theory for the Prediction of Molecular Conformations and Biopolymer Bindings in Solutions with Recent Direct Experimental Tests," *Int. J. Quant. Chem.*, **18**, 381 (1980).

Suffet, I. H., "An Evaluation of Activated Carbon for Drinking Water Treatment," *Am. Water Works Assoc. J.*, **72**(1), 41 (1980).

Sugden, S., "A Relation Between Surface Tension, Density, and Chemical Composition," *J. Chem. Soc.*, **125**, 1177 (1924).

Vedeneyev, V. I., L. V. Gurvich, V. N. Kondrat'yev, and V. A. Medvedev, *Bond Energies, Ionization Potentials and Electron Affinities*, St. Martins Press, New York (1966).

Woodfield, K., "Adsorption of Organic Homologues from Aqueous Solution onto Activated Carbon," Masters Thesis, Rensselaer Polytechnic Institute (1982).

Manuscript received October 5, 1982; revision received March 11, and accepted March 16, 1983.

Characterization of Mixing in Reactor Systems through Analysis of Regional Tracer Dilution Data Obtained with a Gamma Camera

A new approach to the characterization of flow patterns and mixing through analysis of regional tracer dilution data obtained with a gamma camera is presented. Studies performed in a small, two-dimensional, multiple-inlet vessel demonstrate the experimental technique and how data are analyzed to determine the intravessel spatial distribution of fluid deriving from the traced stream. Good agreement is shown between calculated values of the flow distribution and visually observed flow patterns.

F. S. CASTELLANA, M. I. FRIEDMAN, and J. L. SPENCER

Dept. of Chemical Engineering and Applied Chemistry
Columbia University
New York, NY 10027
and
St. Luke's-Roosevelt Hospital Center
New York, NY 10025

SCOPE

While numerous models have been proposed to characterize fluid mixing in reactor vessels (e.g., Weinstein and Adler, 1967; Nishimura and Matsubara, 1970; Goto et al., 1973; Dudukovic, 1977; Spencer et al., 1980), their assessment has been relatively circumscribed due to the limited availability of relevant and detailed experimental data. Recently, it has been shown that

Correspondence concerning this paper should be addressed to F. S. Castellana, Department of Chemical Engineering, Columbia University, New York, NY 10027.

such detailed information may be obtained using radionuclide tracers and a gamma camera (Castellana et al., 1980a). The experimental technique provides a visual description of flow patterns, as well as data characterizing the temporal distribution of tracer within arbitarily defined subregions of a flow system. While the potential of the methodology was established, important problems in data reduction resulting from factors such as camera spatial and temporal nonlinearity, determination of counting efficiency, and Compton scattering were not considered, nor was a theoretical basis for data analysis presented.

The purpose of this paper is to extend the work already presented by: a) detailing experimental and analytical procedures by which quantitative data are obtained; and b) showing an approach to the analysis of these data based on an adaptation of the theory proposed by Castellana et al. (1980b) for linear systems. Quantitative results that describe flow patterns and mixing in a small two-dimensional vessel with two inlet streams will be presented to illustrate the methodology.

CONCLUSIONS AND SIGNIFICANCE

A new approach to the characterization of flow patterns and mixing in reactor vessels through analysis of regional tracer dilution data obtained with a gamma camera has been developed. The theoretical methodology assumes a linear system with time-invariant mixing properties, and develops a relationship from which the fraction of fluid in any vessel subregion (i) deriving from any traced substream (j) may be determined. Designated as a local fraction, B_{ij}, this variable may be used alone, or in conjunction with a model-based analysis, to evaluate mixing, or to assist in characterizing the intravessel distribution of flow, chemical reactants, or heat. Experimental studies in a small two-dimensional vessel demonstrate the technique and relationship between visually observed flow patterns and calculated values of B_{ij}.

Important advantages of the gamma camera imaging system include: a) an ability to collect data simultaneously and in digital form with a spatial resolution of 6–8 mm, or 2–3% of the full field of view, from all points within a two-dimensional projection of the test system; b) the capability of making noninvasive measurements under conditions of elevated temperature and pressure within metallic vessels; c) time resolution in excess of 100 frames per second; and d) an ability to image liquid-, gas- and solid-phase tracers, individually or simultaneously. While the two-dimensional limitation may represent a constraint, the theoretical approach and experimental technique, nevertheless, hold much promise for the characterization of flow patterns and mixing in complex systems.

THEORY

Consider a constant-volume (V) chamber (the system) composed of N constant-volume, perfectly-mixed subcompartments interconnected in an arbitrary way by convective and turbulent transport. [For a general discussion of systems of this type see, for example, Bergner (1961a, 1961b) and Castellana et al. (1980b).] Further, consider M inlet streams each with constant volumetric flow rate Q_j. Each subcompartment receives fluid either directly from an inlet stream or via a path involving other subcompartments. It has already been shown (Castellana et al., 1980b) that if this system is linear with time-invariant mixing properties

$$\int_0^\infty C_i(t)dt = \sum_{j=1}^{M} (W_j/Q_j)B_{ij} \tag{1}$$

where $C_i(t)$ is the time-dependent concentration that would be measured by a detector in subcompartment i, W_j is the total mass of tracer in feed stream j, and the variable B_{ij} is the fraction of fluid in subcompartment i that derives from substream j.

When the tracer is a radionuclide, the measured variable is subcompartment activity (tracer mass), $R_i(t)$, rather than concentration. $R_i(t)$, called in what follows the tracer residue function, is related to concentration by

$$R_i(t) = \alpha_i C_i(t) V_i \tag{2}$$

where α_i is a counting efficiency for the ith subcompartment (counts/s/g), and V_i is the volume of subcompartment i. Note that α_i is a function of detector operating characteristics and geometry, detector-subcompartment orientation, and the composition of the subcompartment medium as well as the medium between the detector and the subcompartment, and is generally unknown.

Consider the case of tracer injection only into inlet stream j. Here, $W_k = 0$, $k \neq j$, and Eq. 1 becomes

$$\int_0^\infty C_i(t)dt = (W_j/Q_j)B_{ij} \tag{3}$$

Using Eq. 2, this expression can be rewritten in terms of the subcompartment tracer residue function, $R_i(t)$

$$\int_0^\infty C_i(t)dt = (1/\alpha_i V_i W_j) \int_0^\infty R_i(t)dt = (W_j/Q_j)B_{ij} \tag{4}$$

Solving for B_{ij}

$$B_{ij} = (Q_j/\alpha_i V_i W_j) \int_0^\infty R_i(t)dt \tag{5}$$

The quantity $\alpha_i V_i W_j$ can be determined from closed system measurements by allowing the injected tracer to recirculate at the end of an experiment until tracer concentration reaches equilibrium within the entire system volume. At equilibrium

$$W_j = C_E V_T = (\overline{R}_i/\alpha_i V_i)V_T \tag{6}$$

and

$$W_j \alpha_i V_i = \overline{R}_i V_T \tag{7}$$

where C_E is the equilibrium concentration of tracer in the total volume of the flow system (V_T), and $\overline{R}_i$ is the activity measured at equilibrium in subcompartment i. Substituting into Eq. 5,

$$B_{ij} = (Q_j/\overline{R}_i V_T) \int_0^\infty R_i(t)dt \tag{8}$$

In a multiple-inlet system, the variable B_{ij}, which lies within the range $0 \leq B_{ij} \leq 1$, is related to intrasystem mixing, and is affected by turbulent and convective diffusion. If mixing in the system is perfect and tracer is injected into any one of the inlet streams, B_{ij} is spatially uniform and equal to Q_j/Q. Spatial nonuniformity of B_{ij}, coincident with a positive or negative departure from the value Q_j/Q, is evidence of incomplete mixing. For the case of a single-inlet stream with flow proportional labelling of injected tracer (e.g., uniform concentration), B_{ij} is unity and independent of intrasystem mixing, and the spatial uniformity of B_{ij} is then a measure of flow proportional labelling of a single-inlet stream.

METHODS

Gamma Camera Imaging System

The imaging system used in this study was a Searle Low Energy Mobile Scintillation Camera (Searle Radiographics, Des Plaines, IL) interfaced to a PDP 11/05 computer (Digital Equipment Corp.,

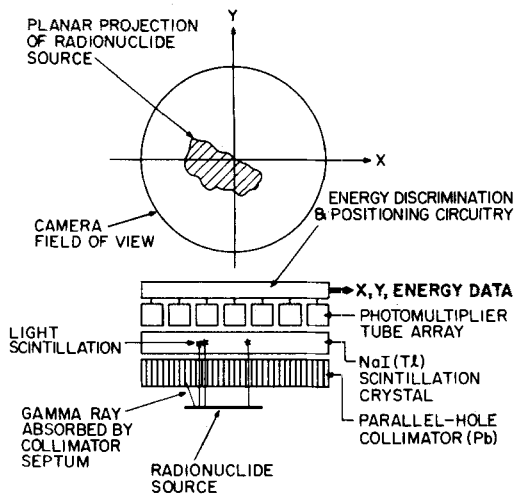

Figure 1. Gamma camera imaging system. Gamma rays normal to the collimator face travelling between the collimator septae interact with the NaI crystal emitting a light scintillation. The *x-y* location of the light scintillation is determined from the weighted output of the photomultiplier tube array by analogy positioning circuitry.

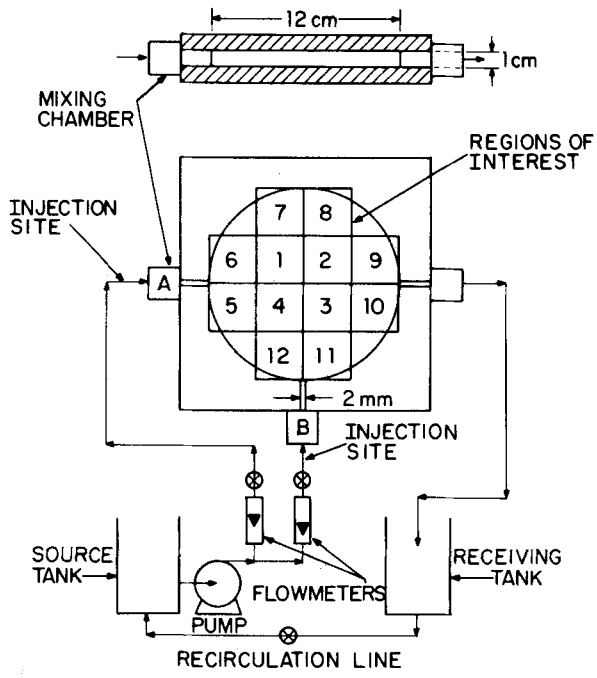

Figure 2. Test reactor and flow system. Each of the 12 regions of interest used in data analysis is composed of 64 pixel elements.

Maynard, MA). The operating characteristics of this system have already been described in detail (Castellana et al., 1980a). In summary, the detector is a 25.7 cm diameter thallium activated NaI crystal above which is an hexagonal array of 37 photomultiplier tubes and below which is a parallel-hole lead collimator (Figure 1). All gamma rays emitted normal to the camera face and passing through the collimator enter the NaI crystal; other gamma rays are stopped by the collimator septae. A scintillation occurs at each interaction, and its location within the crystal is determined from the photomultiplier tube response by appropriate analog circuitry. An upper and lower bound on accepted energies (energy window) can be set to minimize the effects of scattered radiation. (See Discussion.) The data provided by the camera thus comprise a series of *x-y* coordinates recorded at a rate directly proportional to the activity (or mass) of the tracer. Spatial resolution is a function of collimator design, distance of the source to the camera face, and the extent of Compton scattering, but is of the order of 6–8 mm, or 2–3% of the full field of view.

Analysis of the data stream is effected by selecting a "frame time," or counting period, and then storing all of the counts occurring within that period in an N × N matrix (32 × 32, 64 × 64, 128 × 128) according to the *x-y* locations of the counts on the camera face. Selection of the frame time is arbitrary, but in practice is determined by the total count rate and counting statistics errors. Framing rates in excess of 100 per second are possible.

Once the data are framed, activity-time curves (counts/frame-time vs. time) from any subregion of the crystal can be generated by summing count data from appropriate contiguous matrix locations. In practice, the lower bound on subregion size is determined by counting statistics, since the relative error in count rate increases as the size of the subregion decreases.

Test Reactor and Flow System

The gamma camera is well suited to the investigation of flow patterns and fluid mixing in planar geometries; such a geometry was selected for this study, Figure 2. The lucite flow chamber was 12 cm in diameter and 1 cm high, with entrance and exit ports 2 mm wide, 1 cm high,and 2.5 cm long. The flow system was designed for one or two inlet operation with a single exit stream; distilled water was used as the fluid. The tracer injection site was located 10 cm proximal to the inlet, and injection was through a 1.25 mm diameter tube with a closed end and two-side holes oriented 180 degrees apart and transverse to the direction of flow. To assure flow proportional labelling of the inlet stream, a 2.5 cm diameter × 2 cm long chamber containing three screens located perpendicular to the flow was placed between the injection site and the test chamber in apposition to the entrance slit. The purpose of the screens and the sudden contraction was to assure complete mixing of tracer and a flat velocity profile in the entrance stream. The flow system was designed for single-pass operation, with a capability of interconnecting source and receiving tanks for measurements of equilibrium activity at the end of each experiment. A centrifugal pump with a manifold and valve system was employed to achieve desired flow rates, which were measured by two rotameters.

Tracer Studies with Single- and Two-Inlet Flow

Assessment of Flow-Proportional Labelling in the Traced Stream. It has been shown that the integral of the tracer residue function is independent of location in the vessel for conditions of flow-proportional labelling. This criterion was used to assess the ability of the injection system to provide flow-proportional labelling of the traced stream. Three experiments were conducted for single-inlet flow conditions, over a flow range 0.92 to 3.26 L/min, with the test vessel placed on top of, and in apposition to, the collimator of the gamma camera.

In each experiment, the flow rate was set, the data acquisition started, and 15–20 mCi of 99m-Technetium pertechnetate (140 keV gamma emitting radionuclide with a half-life of 6 hours) in a fluid volume of approximately 0.50 mL was injected rapidly (over a period of 1 to 2 seconds) into the inlet stream. Data were collected for time periods of up to 1 min, and in all cases the collection period was in excess of eight mean transit times. Upon termination of data collection, flow was allowed to recirculate until measured activity in the test vessel was constant. Equilibrium activity data were then recorded and stored for processing. In each experiment, a marker source with an activity between 6,000–7,000 cps was placed in the camera field of view in apposition to the collimator. The purpose of the fixed source was to characterize and allow correction for camera count rate nonlinearity at high count rates.

Fluid Mixing with Two-Inlet Streams. Studies of fluid mixing within the reactor were conducted with flow through both inlets. In two experiments, the flows through inlets A and B (Figure 2) were set equal, and in a third experiment the flow through inlet A was set equal to twice that through inlet B. In the first two experiments, tracer was injected into stream A, and in the third into

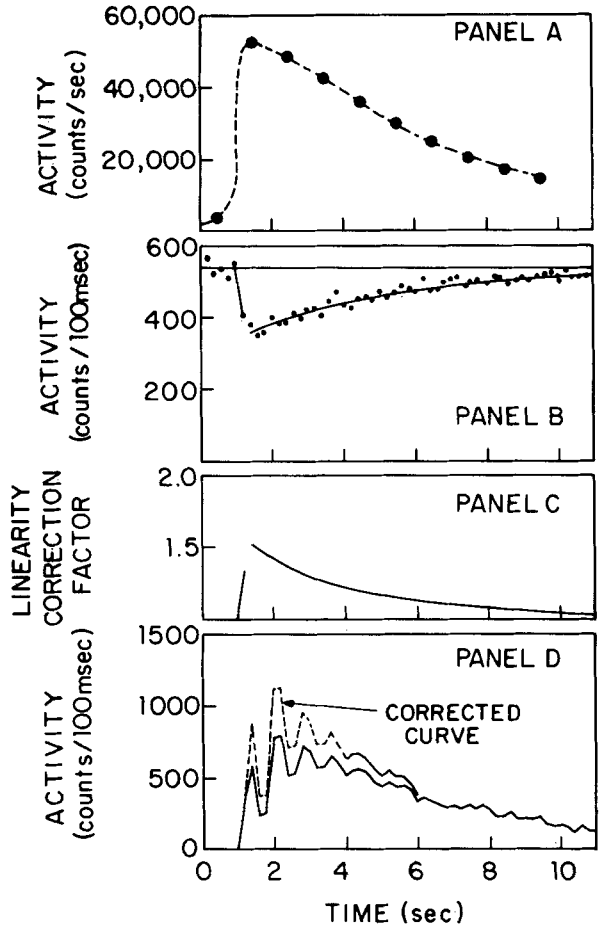

Figure 3. Correction for camera nonlinearity at high count rates: Panel A—total crystal count rate; Panel B—marker source activity; Panel C—correction function; Panel D—original and corrected data for a typical region of interest.

stream B. In each case, the experimental protocol was as outlined for the single-inlet studies.

Data Analysis

Region-of-Interest Selection and Correction for Camera Nonlinearity at High Count Rates. A 64 × 64 framing matrix was selected for data analysis. The vessel volume was viewed through 12 identical square regions-of-interest each containing 64 pixels (Figure 2). With this region-of-interest definition, the volume viewed by subregions 1, 2, 3 and 4 was 10.3 cm^3 (3.21 cm × 3.21 cm × 1.0 cm high), and that viewed by subregions 5, 6, 7, 8 and 9 was 9.88 cm^3. To improve counting statistics for this analysis, border pixel elements in contiguous subregions were defined as contributing to both subregions. An additional region-of-interest was placed over the marker source for the purpose of evaluating and correcting for camera count-rate nonlinearity with source activity at high count rates (in excess of 25,000 per second). A frame time of 100 or 200 ms was selected (the shorter frame time was employed at the highest flows), and the variation of the marker source count rate with time fit statistically to an exponential function which was used to correct all data in each of the 12 regions-of-interest as described below.

Calculation of B_{ij}. A value of B_{ij} from Eq. 8 was calculated for each subregion in each of the six experiments. The integral of the residue function for subregion i was determined by summing all the counts in subregion i over the duration of the experiment. The value of the equilibrium activity, $\bar{R}_i$, was that determined from equilibrium measurements at the end of each experimental run. Total system volume (V_T) was determined from an independent measurement, and the flow rate of the traced stream from the setting of the appropriate rotameter.

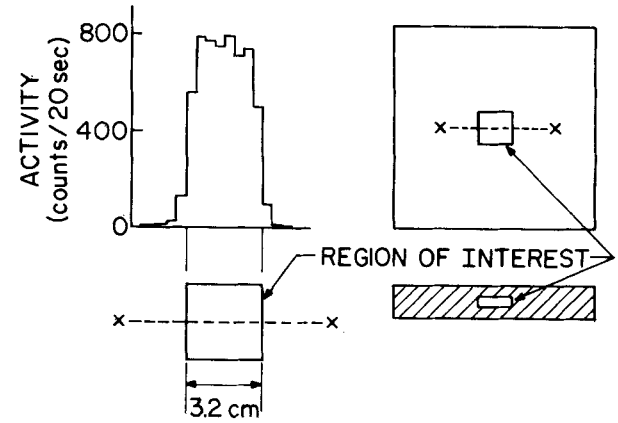

Figure 4. Evaluation of Compton scattering. Shown is the variation of activity along the axis of a cavity filled with a solution of 99-m-Technetium pertechnetate in water and having the dimensions of a region of interest.

Evaluation of Compton Scattering

To estimate the magnitude of Compton scattering, a lucite phantom was constructed with a cavity equal in configuration, location and volume to that of a single subregion. The cavity was filled with a solution of 99-m-Technetium pertechnetate in water, placed on the gamma camera in apposition to the collimator, and activity measurements were recorded.

RESULTS

Characteristics of the Gamma Camera Imaging System

Count Rate Linearity. Gamma camera count rate linearity with source activity at high count rates is affected not only by the absolute count rate, but also by the number of scattered events and by the spatial distribution of the source within the field of view. For this reason, a dynamic calibration during the actual experiment is necessary. The measured activity of the marker calibration source, and the coincident total crystal count rate during a typical experimental run are shown in Figure 3. The system was approximately linear to a count rate of 25,000 per second. At the peak count rate of 52,000 per second, the measured marker source count rate was approximately 67% of its actual value. To effect a count rate correction and to minimize the effects of counting statistics, a straight line was fit to data representing the initial drop in marker count rate, and an exponential function was fit to data representing the subsequent rise. All data in each subregion were then corrected point by point by multiplying the original count rate by the ratio of the preinjection marker count rate for the best fit marker count rate at the respective time. The correction function and original curves for a typical subregion are shown in Figure 3.

Measurements of Compton Scattering. The magnitude and significance of Compton scattering as determined from the phantom study is shown in Figure 4 as a plot of activity vs. distance in a transverse direction along the axis of the subregion. It is observed that only 4.7% of counts actually originating in the simulated subregion appear to originate in a contiguous subregion. Because of this low value of the scatter fraction, no data correction procedures (see Discussion) were applied.

Tracer Studies with Single and Two-Inlet Flow

Panels A and B of Figure 5 show sequential images of the tracer as it flows through the single and two-inlet flow configurations. The frame time as well as the interval between frames is indicated in the figure. The symmetrical recirculating flow pattern evident in Panel A is clearly absent in Panel B. Count data from several representative regions of interest in the two-inlet study are shown plotted as a function of time in Figure 6 at a framing interval of 100 ms. Calculated values of B_{iA} for the single-inlet study and B_{iB} for the two-inlet study are shown for each subregion in Figure 7.

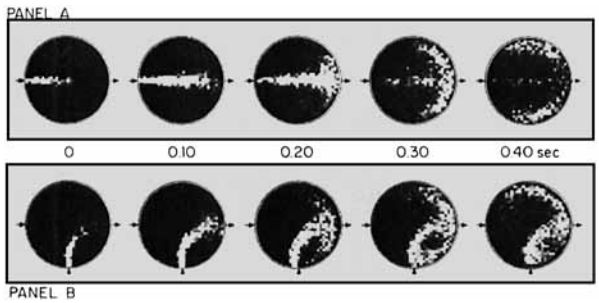

Figure 5. Sequential frames showing radionuclide passage through single- (Panel A) and two-inlet (Panel B) flow configurations. Frame time is 100 ms. Panel A—Q_A = 2.1 L/m, Q_B = 0; Panel B—Q_A = 2.5 L/m, Q_B = 1.25 L/m.

In the single-inlet study, the relatively small deviation of B_{iA} from unity is evidence of flow proportional labelling of the inlet stream. The average values of B_{iA} for each of the three flow rates studied are shown in Table 1, along with the inlet stream Reynolds number, the mean transit time (V/Q), the standard deviation of $\overline{B}_{iA}$, and the value of the largest positive and negative fractional deviation from $\overline{B}_{iA}$. In the two-inlet studies, significant local departures from the "perfect mixing" value of 0.33 are observed. It is seen that B_{iB} is high in subregions 3, 10 and 11, and low in 4, 5 and 12. This corresponds to the distribution of flow observed visually in Figure 5. Results from this study as well as the two-inlet studies with equal inlet flows are summarized in Table 1. It is observed that both the S value and the maximum positive and negative deviation from $\overline{B}_{ij}$ are significantly greater than those in evidence in the single-inlet studies.

DISCUSSION

Region-specific tracer dilution data derived from studies in multiple inlet systems may be analyzed according to the proposed methodology to yield spatial distributions of fluid deriving from any traced stream. Designated as a local fraction (B_{ij}) this variable may be used to evaluate mixing, or to assist in characterizing the distribution of chemical reactants or heat in a specific flow system. The usefulness of this approach is predicated on the availability of detailed experimental data describing the spatial distribution of the time-dependent intrasystem concentration. We have demonstrated that such data may be obtained using readily available radionuclide tracers and a quantitative gamma camera imaging system. Important features of this system include: a) an ability to collect data simultaneously and in digital form with a spatial resolution of 6–8 mm, or 2–3% of the full field of view, from all points within the two-dimensional projection of a reactor vessel; b) the capability of making noninvasive measurements under conditions of elevated temperature and pressure in metallic chambers; c) time resolution in excess of 100 frames per second; and d) an ability to image liquid-, gas- and solid-phase tracers, individually or simultaneously.

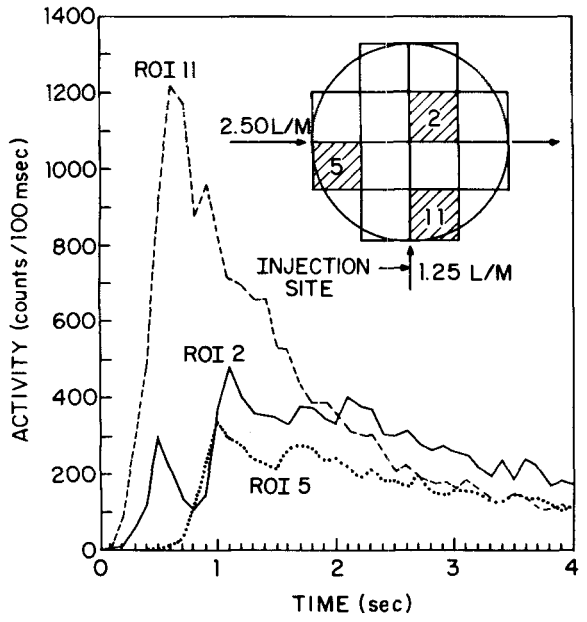

Figure 6. Activity vs. time curves from selected regions of interest (shown cross-hatched) for the two-inlet flow configuration. Frame time is 100 ms.

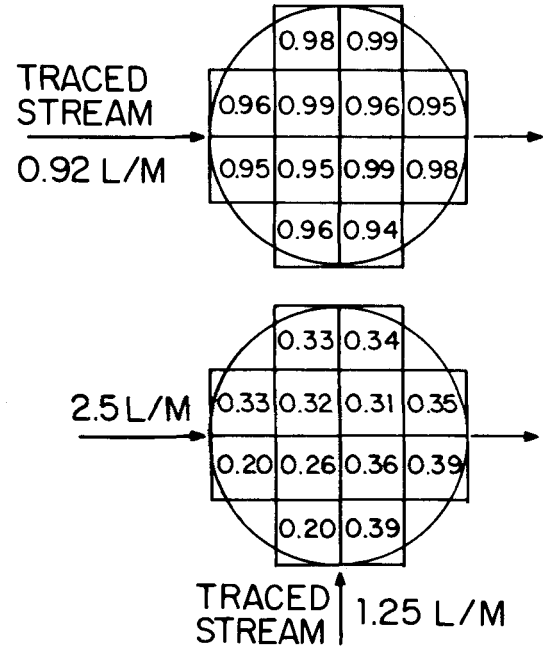

Figure 7. Calculated values of B_{iA} (Panel A) and B_{iB} (Panel B) from Eq. 8 for the experiments shown in Figure 5.

The theoretical development assumes a linear system with time-invariant mixing properties. The variable B_{ij} is the fraction of fluid in subregion i deriving from substream j. This variable does not allow calculation of absolute flow rates, but rather reflects the overall effect of the mixing process. Thus, for example, in a multiple inlet system where each inlet stream is designated by a defined flow rate and specific enthalpy (h_j), the local enthalpy distribution is given by the relation

$$h_i = \sum_{j=1}^{M} h_j B_{ij} \tag{9}$$

In a similar fashion, for each inlet stream containing a single chemical species (a) at a concentration C_j^a, the local concentration distribution of that species is given by

$$C_i^a = \sum_{j=1}^{M} C_j^a B_{ij} \tag{10}$$

In both examples, the development assumes that the measured quantity (heat and mass) enters or leaves the defined region only by a flow process. If an additional transport mechanism is available, such as heat conduction or chemical reaction, Eqs. 9 and 10 no longer hold, and prediction of local enthalpy or concentration requires knowledge of local flow rates.

In the analysis presented, only the integral of the tracer residue function is employed to evaluate the variables B_{ij}, and thus some information contained in the residue functions is not used. Correspondingly, an examination of special cases shows that different intersubcompartment flow rates can produce identical values for B_{ij}. Although B_{ij} is clearly related to the nature of mixing in the flow system, and particularly to the characterization of departures from perfect mixing, the possibility of a more complete analysis of the tracer residue functions is manifest. Such an analysis would determine the basic variables which characterize the state of the

TABLE 1. EXPERIMENTAL CONDITIONS AND CALCULATED RESULTS FOR EACH OF SINGLE- AND TWO-INLET STUDIES

Run	Re_A	Re_B	V/Q (s)	$\bar{B}_{ij}$	S	$D(+)$	$D(-)$
1	1,530	0	7.38	0.97	0.018	0.027	0.027
2	3,450	0	3.28	0.98	0.020	0.030	0.023
3	5,430	0	2.08	1.02	0.031	0.040	0.030
4	770*	770	7.38	0.48	0.036	0.119	0.115
5	1,530*	1530	3.69	0.47	0.035	0.195	0.062
6	4,170	2080*	1.81	0.32	0.064	0.233	0.363

The subscript j refers to the single traced stream denoted by an asterisk in runs 4, 5, and 6.
$\bar{B}_{ij} = \Sigma B_{ij}/12$
$S = (\Sigma(B_{ij} - \bar{B}_{ij})^2/11)^{1/2}$
$D(+) = (B_{ij}(\max) - \bar{B}_{ij})/\bar{B}_{ij}$
$D(-) = (B_{ij}(\min) - \bar{B}_{ij})/\bar{B}_{ij}$

mixing process, namely the intersubcompartment flow rates.

Data available from a single gamma camera are two-dimensional, and measured intensity at any x-y location represents an integral of activity at that location in a direction normal to the crystal face. Three dimensional data are potentially available using multiple camera imaging systems, or by assuming stationarity and imaging the process several times with one camera at different orientations.

Primary gamma rays undergo both attenuation and Compton scattering. Attenuation affects the activity coefficient, and is accounted for in equilibrium activity measurements made at the end of a study. Because of Compton scatter, primary gamma rays may appear to come from a subregion from which they in fact did not originate. The scattering results in both a loss of energy and change in direction for the affected gamma ray. The relationship between the energy of the scattered gamma ray and the angle of scatter is given by (e.g., Semat, 1958)

$$E_s/E_i = 1/(1 + (E_i/511)(1\text{-}\cos\theta)) \qquad (11)$$

Here, E_s and E_i are, respectively, the energy (keV) of the scattered and incident gamma rays, 511 keV is the rest mass energy of an electron, and θ is the angle between the direction of the primary and scattered rays. For a 99-m-Tc energy window of ± 10%, all interactions with an angle of scatter greater than 60 degrees are eliminated. However, even with this constraint, the geometric configuration of this study permits a primary gamma ray originating at the top of the reactor to be measured as an event at a location 1.6 cm from its origin. The actual magnitude and location of the scattered events can be determined experimentally as described, or calculated using a Monte Carlo technique (Raeside, 1976).

As already demonstrated, for the regions of interest used in this study, scattering has minimal significance. As the selected regions of interest decrease in size, however, scattered photons assume increased importance and must be taken into account. A correction to the measured region-of-interest activity can be generated from studies using phantoms. The fractional contribution of scattered radiation from primary to contiguous subregions can be determined experimentally, and the following set of simultaneous equations solved for each frame of the study for primary subregion activity.

$$A_{im} = A_i + \sum_{i \neq j} k_{ij} A_j \qquad (12)$$

Here, A_{im} is the measured activity in subregion i, A_i is the activity due to tracer in subcompartment i, k_{ij} is the fractional contribution to the measured activity in subregion i of tracer located in subcompartment j, and A_j is the activity due to tracer in subcompartment j.

Camera nonlinearity becomes important at count rates in excess of 20,000–25,000 per second. Nonlinear behavior results from the finite time required to analyze and process each scintillation. Since scintillations of all energies are detected and analyzed, including those scattered events occurring outside of the energy window, nonlinearity calibrations must be made from data derived during the study. The performance of the camera used in this study is typical of available instruments. The peak count rate for any study is determined by subregion size and the desired time response. Improving spatial resolution by decreasing subregion size, or improving time response by increasing the framing rate, decreases the number of counts per subregion per frame. Since gamma decay follows Poisson counting statistics, (the standard deviation of the count rate is given by the square root of the count rate divided by the count rate) the minimum number of counts required for a specific degree of accuracy is easily determined. In these experiments, peak subregion count rates were of the order of 1,500–2,000 per 200 ms frame. The error incurred in evaluating the integral of the activity-time curve is, of course, significantly less than that associated with any single point because of the increased number of measured counts.

Increased resolution of the spatial variation of B_{ij} could be obtained by decreasing subregion size without a significant increase in statistical counting errors. Thus, for example, in experiment 5 the average subregion value of the integral of the activity-time curve was approximately 39,000, with a standard deviation of ±0.51%. If the number of subregions were increased by a factor of four, the standard deviation of the integral would increase to ±1.01% (assuming that the average value of the integral decreased by a factor of four). Significant decreases in subregion size would require corrections for Compton scattering as already outlined.

In summary, subregion activity-time data as well as the spatial distribution of B_{ij} can be used in conjunction with a model-based analysis for evaluation of mixing and other transport parameters. While the two-dimensional limitation may represent a constraint, the theoretical approach and experimental technique, nevertheless, holds much promise for the characterization of flow patterns and mixing in complex systems.

LITERATURE CITED

Bergner, P. E., "Tracer Dynamics: I. A Tentative Approach and Definition of Fundamental Concepts," *J. Theoret. Biol.*, **2**, p. 120 (1961a).

Bergner, P. E., "Tracer Dynamics: II. The Limiting Properties of the Tracer System," *J. Theoret. Biol.*, **1**, p. 359 (1961b).

Castellana, F. S., J. L. Spencer, and A. Cartolano, "Application of the Gamma Camera to Studies of Flow and Mixing in Reactor Vessels," *Ind. Eng. Chem. Fund.*, **19**, p. 222 (1980a).

Castellana, F. S., S. M. Snappin, S. Y. Tam, and R. B. Case, "Inlet and Intrachamber Concentration Distributions in Tracer Studies of the Canine Central Circulation and Their Relation to the Isotope Dilution Residue Function," *Circ. Res.*, **47**, 10 (1980b).

Dudukovic, M. P., "Micromixing Effects on Multiple Steady States in Stirred-Tank Reactors," *AIChE J.*, **23**, p. 382 (1977).

Goto, S., Y. Nishimura, and M. Matsubara, "Relation Between the Two-Environment Model and the Accumulator Model for Micromixing in Continuous Flow Systems," *Chem. Eng. Sci.*, **28**, p. 1498 (1973).

Nishimura, Y., and M. Matsubara, "Micromixing Theory via the Two-Environment Model," *Chem. Eng. Sci.*, **25**, p. 1785 (1980).

Raeside, D. E., "Monte Carlo Principles and Applications," *Phys. Med. Biol.*, **21**, p. 181 (1976).

Spencer, J. L., R. L. Lunt, and S. A. Leshaw, "Identification of Micromixing Mechanisms in Flow Reactors: Transient Inputs of Reactive Tracers," *Ind. Eng. Chem. Fund.*, **19**, p. 135 (1980).

Semat, H., *Introduction to Atomic and Nuclear Physics*, Rinehart & Co., Inc., New York (1958).
Weinstein, J., and R. J. Adler, "Micromixing Effects in Continuous Chemical Reactors," *Chem. Eng. Sci.*, **22**, p. 65 (1967).

NOTATION

A = activity of radionuclide tracer
B_{ij} = fraction of fluid in subcompartment i that derives from substream j
C = concentration
E = gamma ray energy
h = enthalpy
Q = flow rate
R = residual tracer activity
t = time
V = volume
w = mass rate of tracer flow
W = total tracer mass
α = counting efficiency constant
θ = angle of gamma ray scatter

Subscripts

E = equilibrium
i = subcompartment designator
j = flow stream designator
T = total system

Manuscript received October 30, 1981; revision received April 15 and accepted April 29, 1983.

Hydrodynamics and Mass Transfer in Non-Newtonian Solutions in a Bubble Column

Until now the oxygen transfer in viscous non-Newtonian solutions has been studied only in bubble columns of about 0.14-m diameter. Recently Godbole et al. (1982) reported much smaller gas holdups in Carboxy Methyl Cellulose solutions (CMC) for a large-diameter column. Therefore, the gas holdups, volumetric mass transfer coefficients, and specific gas-liquid interfacial areas are measured in CMC solutions using a bubble column of diameter 0.305 m and height 3.4 m. The transition from churn-turbulent to slug flow regime occured at higher viscosities and the gas holdups and volumetric mass transfer coefficients were lower in both flow regimes than reported for smaller column diameters. Empirical correlations are presented for the gas holdup, volumetric mass transfer coefficient, and specific gas-liquid interfacial area which would be suitable for the design of fermentors.

S. P. GODBOLE, A. SCHUMPE, and Y. T. SHAH

Chemical and Petroleum Engineering Department
University of Pittsburgh
Pittsburgh, PA 15261
and

N. L. CARR

Gulf Research and Development Co.
Harmerville, Pittsburgh, PA 15230

SCOPE

Bubble column reactors are becoming increasingly popular in the biotechnological and pharmaceutical industry. The rheological behavior of microbiological cultures in a fermentation tower can be fairly well simulated by the solutions of carboxymethyl cellulose (CMC). All the literature data for the hydrodynamics and mass transfer in CMC solutions were taken in columns of up to 0.14-m diameter. Recently for viscous CMC solutions, Godbole et al. (1982) reported a strong decrease in the gas holdup with an increase in the column diameter. The strong dependency of the gas holdup on column diameter suggests a similar dependency for the volumetric mass transfer coefficient, i.e., the previous investigations in columns of 0.14-m diameter are insufficient for scale-up purposes. The correlation of Nakanoh and Yoshida (1980) even suggests an increase in volumetric mass transfer coefficient with increasing column diameter. Therefore, in this work oxygen mass transfer in CMC solution was studied in a 0.305-m diameter column.

Volumetric mass transfer coefficients are measured by the dynamic method. Specific interfacial areas are determined by the sulfite oxidation technique used by Schumpe and Deckwer (1982). The kinetics of the cobalt catalyzed reaction is not affected by addition of CMC (Wesselingh and van't Hoog, 1970); Onken and Schalk, 1978; Poggemann, 1982) and the deviation of the chemically effective interfacial area from the geometrical one is small because of the small gas-phase conversion (Schumpe and Deckwer, 1980a,b). The gas holdups are measured using a hydrostatic head technique and fractional gas holdups are measured using the dynamic gas disengagement technique (Sriram and Mann, 1976). To study the influence of the added salt, volumetric mass transfer coefficients are determined in CMC/sodium sulfate solutions and compared with the k_La values obtained in pure CMC solutions. Fermentation media might be more complex than the model media used and hence the effect of surfactant (Triton X-114) on the hydrodynamics and mass transfer in CMC solutions is studied. The gas holdup, volumetric mass transfer coefficient, and gas-liquid interfacial area are correlated empirically. These correlations are based on data collected in a large-diameter column for wide ranges of gas throughputs and apparent liquid-phase viscosities and hence would be better suited for the scale-up of fermentors than those presently available.

A. Schumpe is currently with the Techn. Chemie, FB 9, Univ. Oldenburg, Oldenburg, W. Germany.